6th International Conference on Water Resources and Arid Environments (ICWRAE 6): 288-297
16-17 December, 2014, Riyadh, Saudi Arabia

Integrated Geophysical Interpretation for Groundwater Exploration at the Central Part of Sinai, Egypt

[1]Sultan Awad Sultan Araffa, [2]Hassan M. El Shayeb, [2]M.F. Abu-Hashish and [2]Noha M. Hassan

[1]National Research Institute of Astronomy and Geophysics, Helwan 11722, Cairo, Egypt
[2]Faculty of Science, Menoufia University, Egypt

Abstract: In the present study three geophysical techniques (Land gravity, electrical resistivity and land magnetic) have been applied to identify and evaluate the groundwater occurrences in the studied area, which lies between latitudes 29° 18` and 29°52` N and longitudes 33° 25` 34°32` E. Twenty six deep VES stations were measured and interpreted to delineate the Nubian sandstone aquifer in the area. The upper surface of the aquifer varying from 483 to 1079 m and the resistivity values ranging from 109 to 522 Ohm-m which represents the fresh water aquifer in the study area. The results of gravity interpretation indicate that the area dissected by different fault elements of different directions such as NE-SW trend parallel to the Gulf of Aqaba, NW-SE trend parallel to the Gulf of Suez and E-W trend parallel to the Mediterranean Sea. The depth of basement rocks ranging from 2100 to 4300 m.

Key words: Groundwater aquifers · Geophysical tools · Schlumberger configuration

INTRODUCTION

Sinai Peninsula covers an area of about 61.000 km^2. It is bounded by the Gulf of Suez, the Suez Canal from the western side and the Gulf of Aqaba from the eastern side. It is part of the Asiatic continent extending over a distance of 200 Km between Rafah on the Mediterranean Sea and Taba at the Head of the Gulf of Aqaba.

The water scarcity is a major socio-economic crisis in Sinai Peninsula of Egypt. Lack of proper water resources planning led to the drastic dropdown in Sinai urbanization and population development. Drought management, as well as sustainable agricultural production in arid and semiarid areas of Sinai deserts will depend heavily on meticulous planning in the exploration, exploitation and utilization of water resources for favoring the human requirements.

The agrarian system in Wadi El-Arish delta and the coastal belt in northern Sinai have a large extent, rainfall dependent, which in turn is highly erratic in nature.

This calls for an intervention of a framework where Remote Sensing (RS), Geographic Information Systems (GIS) and watershed modeling tools could be useful in determining potential areas for Rainwater Harvesting (RWH). Planning should be based on the drainage basins, where effective methodologies and systematic information on the resources base are obtained to quantify, analyze and formulate targets of water resources development by RWH.

The groundwater resources in Sinai are relatively renewed by the sporadic rainfalls and flash floods occurring at its southern parts during the transitional periods between Spring and Autumn. Furthermore, groundwater recharge or deep drainage percolation is a hydrologic process where rainwater moves downward to the groundwater. Geophysics has been long used for a wide variet y of groundwater exploration problems as in] [1-3].

This study is mainly conducted to identify the groundwater occurrences in the studied area (Figure 1), to determine different structural elements which dissect the studied area and to define the basement complex depth and thickness of the sedimentary cover.

Wadi Yarqa Abu Taryfya is one of the most important tributaries of of Wadi El- Arish. Many geophysical investigations have been carried out around the studied area [4-6].

Corresponding Author: Sultan Awad Sultan Araffa, National Research Institute of Astronomy and Geophysics, Helwan 11722, Cairo, Egypt.

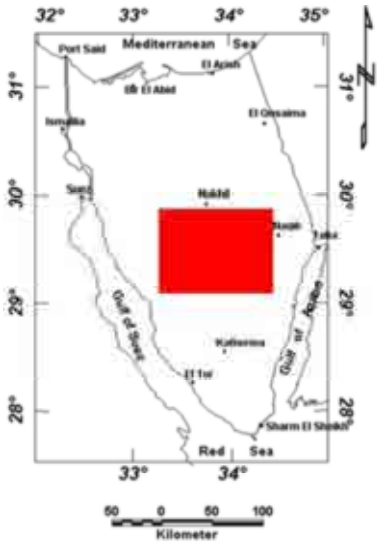

Fig. 1: Location map of the studied area

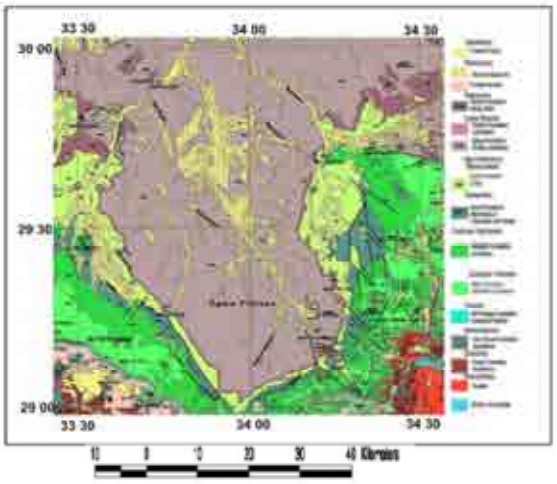

Fig. 2: Geological map of the studied area (modified after UNISCO, Cairo office 2004)

The studied area comprises Wadi Yarqa Abu Taryfya and its tributaries, as well as, its junction with Wadi El-Arish. It covers a surface area of about 5395 km^2 between latitudes 29° 18` & 29° 52`N and longitudes 33° 25` & 34° 32` E.

Geological Setting: Geomorphology: the studied area is built up of nearly horizontal to slightly tilted strata ranging in age from the Paleozoic Era at the south to the Cenozoic Era at the north. El Egma plateau represents one of the most principal watershed areas in Sinai. It is built up of northward gently dipping strata which are mainly composed of Lower Eocene Limestone with chert bands.

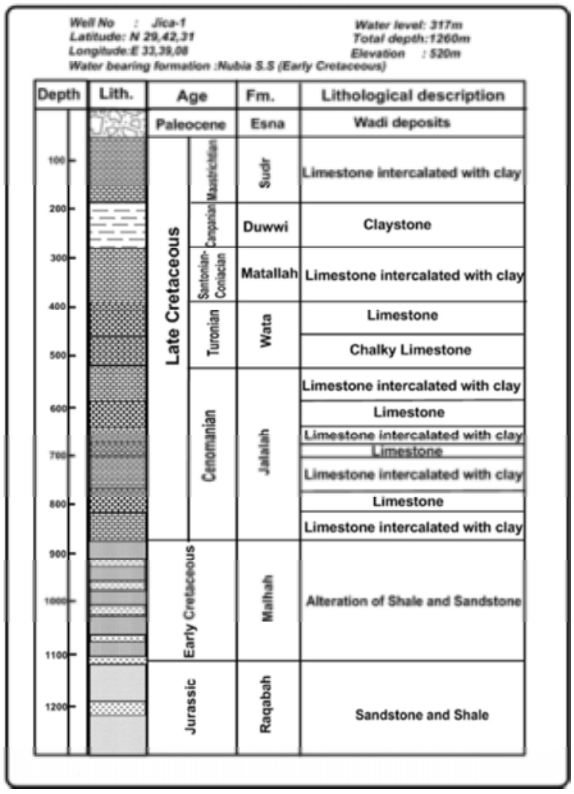

Fig. 3: Lithostratigraphic sequence of Jica well No.1 (after Jica, 1992)

The basal portion of its escarpment is composed of massive Upper Cretaceous chalk. The eastern extension of El Egma tableland to the northwest, is dissected by numerous hilly and mountainous terrains. The eastern part of this unit has ground elevation of about 1000 m which is reduced northward at Shaeira plain to about 700 m. It is occupied by mountains and hills of sedimentary rocks [7].

Stratigraphy: The outcropping rock units in the studied area are the, Cambrian, Jurassic, Cretaceous, Paleocene Lower Eocene, Pliocene and Quaternary in age (Figure 2). The subsurface lithostratigraphic succession was obtained from the existing and nearby wells as in Jica well No 1. (Figure 3) shows the subsurface lithostratigraphic column which reaches a drilling depth of about 1260 m [8].

Geoelectrical Measurements and Interpretation

Ves Stations Interpretation: The geoelectrical studies in the present studied area, is represented by 26 vertical electrical soundings (VES) as shown in (Figure 4). The field survey has been carried out by application of

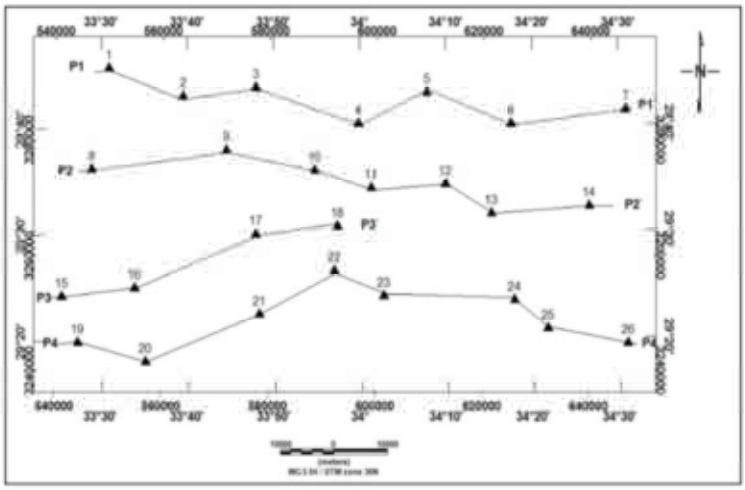

Fig. 4: Location map of the vertical electrical sounding and the selected profiles along 1Dresistivity cross-sections are constructed

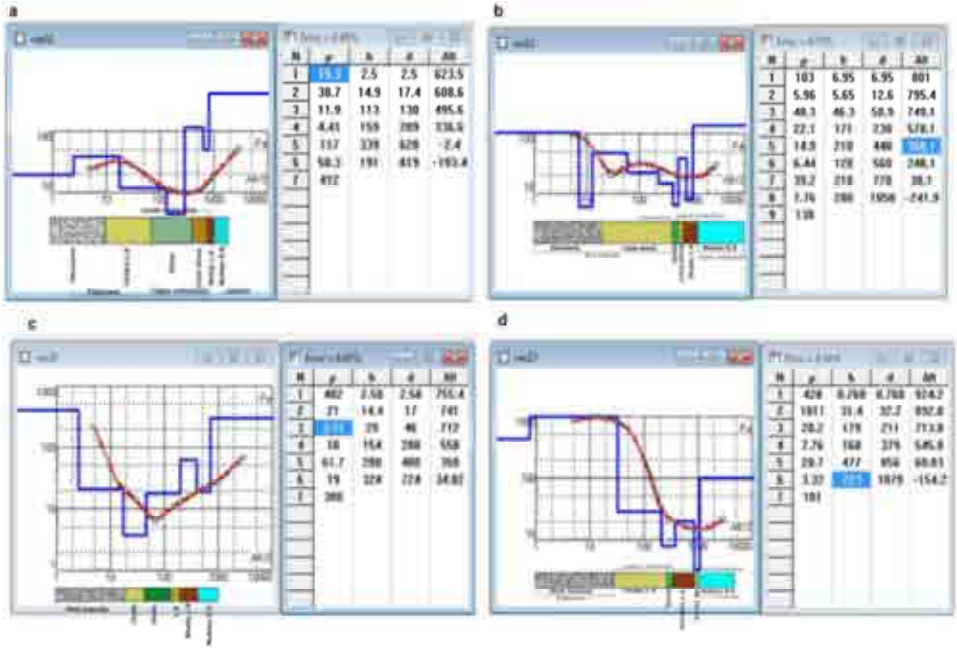

Fig. 5: Resistivity models for Veses (a) ves2, (b) ves11, (c)ves 20 and (d) ves 23 and its correlation with the geological logs obtained from the boreholes Jica 1,2,6 and 4 respectively

the standard Schlumberger electrode configuration with AB/2 spacing varying logarithmically from 5 meters to 3000 meters. These VESes are arranged more or less in a grid-like pattern, about 2 km apart, along N-S and E-W trending lines according to the simple terrain to provide a reasonable coverage of the studied area. To verify the geophysical interpretation results, JICA 1, 2, 6 and 4 respectively close to VESes 2, 11, 20 and 23 whose lithologic and/or well logging data are available.

The quantitative interpretation of vertical electrical soundings was carried out using a graphical method based on the two layer curves and the generalized Cagniard graphs Koefoed (1960). The results of manual interpretation were used as the initial models for theIPI2WIN-1D Program (2007) software in order to compute the true depths and resistivities of the one dimensional model for each VES curve (Figure 5). This program uses a linear filtering approach for the forward

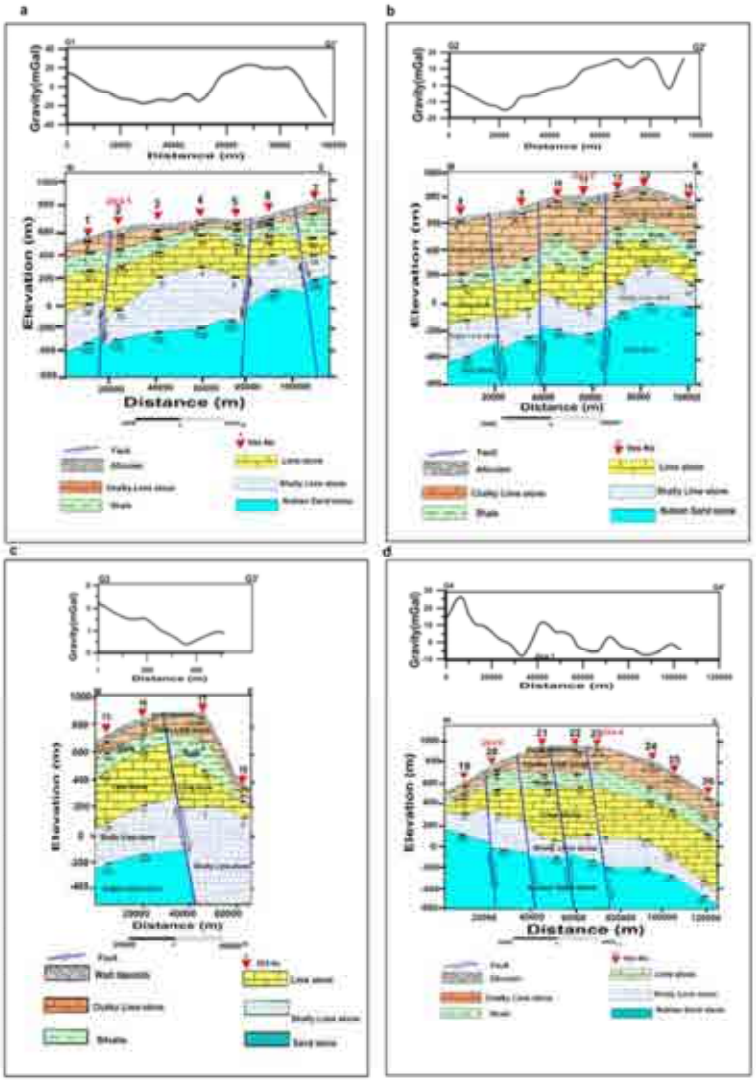

Fig. 6: 1D Geoelectric cross-section along profiles (a). P1 (b). P2 (c). P3 and (d).P4 compared with gravity profiles

calculation of a wide class of geological models, depending upon regularized fitting minimizing algorithm using Tikhonov's approach [9-11].

Geoelectric Cross-Section: The results of VES interpretation are used to construct four geoelectric sections, P1, P2, P3 and P4 as shown in (Figure 6) respectively.

The geoelectric cross-sections exhibit six geoelectric units: The first unit is the Quaternary alluvial deposits with thickness values ranging from 2.12m to 40 m and resistivity values varying from29 Ohm-m to 498.9 Ohm-m. The second unit is Limestone with Upper cretaceous, Maastrichtian (Sudr Formation) with thickness values ranging from 15.3m to 427m and resistivity values ranging from 3.72 Ohm-m to 165.4Ohm- m. The third unit is Shale with Upper cretaceous, Campanian and Santonian (Matallah Formation), with thickness values ranging from 18.6 to 289 m and resistivities ranging from 3.3 to 46.2 Ohm-m. The fourth unit is composed of Limestone which belongs to Coniacian-Santonian and Turonian (Wata Formation) and changes laterally towards east to Dolomitic Limestone with the same age, with resistivities ranging from 9.3 to 216 Ohm-m and thickness values ranging from 117 to 477 m. The fifth unit is composed of highly fractured dolomitic Limestone, Shalley Limestone, marls, Shales, of Cenomanian age with resistivity values ranging from2.14 to 54.6 Ohm-m and thickness values varying from 120 to 512 m. The sixth unit is the last detected unit.

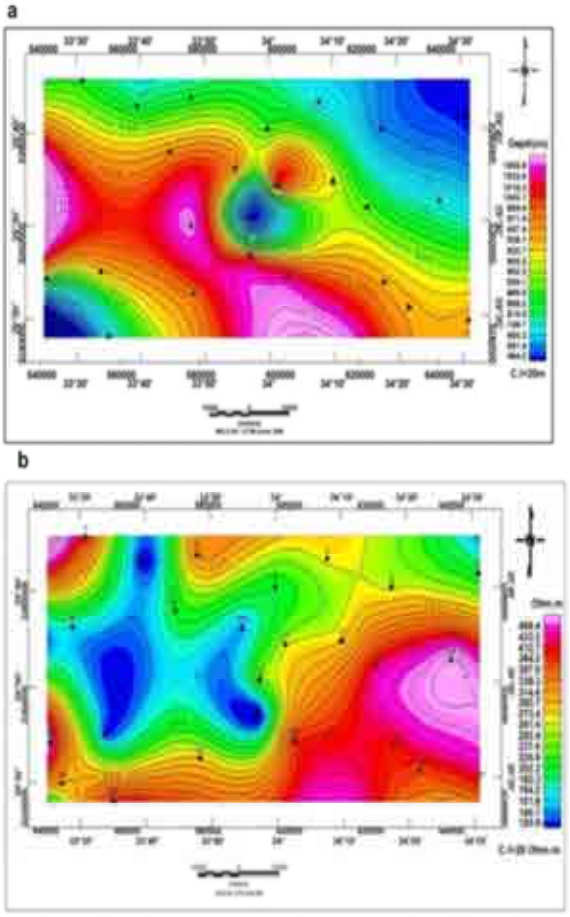

Fig. 7: (a) Depth map of Nubian sandstone aquifer (b) Isoresistivity map of Nubian sandstone aquifer

The upper surface of this layer has been pronounced at depths varying from 483 to 1079m while the lower surface cannot be reached, by the used geometry of electrode configuration. It is formed of thick bedded grained Sandstones (Nubian sandstone) Lower cretaceous (Malhah Formation) to Jurassic age with resistivity values ranging from 109 to 522 Ohm-m which represents the fresh water aquifer in this area.

Depth Map of Nubian Sandstone Aquifer: The depth map of the Nubian Sandstone aquifer shows shallow depths at the northeastern part and southwestern part of the studied area (460 - 800 m) but the southern part extending from central to western part exhibit deep depth about (920-1060m) as shown in (Figure 7a).

Isoresistivity Map of Nubian Sandstone Aquifer: Isoresistivity map of the sixth geoelectrical unit shows that the whole area is represented by high resistivity range from (260 to 500 Ohm.m) While the small part of western corner represented by low resistivity range from (120 to 200 Ohm.m). This layer is composed of Sandstone of Lower Cretaceous aquifer (Nubian Sandstone) as shown in (Figure 7b).

Table 1: Correlation factor for different orders

Order	Value
r 1-2	0.4388
r 2-3	0.8431
r 3-4	0.6661
r 4-5	0.9996

Gravity Measurements and Interpretation: Gravity data has been acquired by the *CG-3 Gravimeter* through 211 land stations arranged in a grid-like pattern, 500 m apart, to cover the whole area of sensitivity of 0.01 mGal. The measured gravity values were corrected to different gravity corrections such as drift, tide, free-air, Bouguer, latitude and topographic corrections using specialized software (Geosoft 2007). The corrected gravity values were used to plot Bouguer anomaly map using Oasis Montaj 2007 as shown in (Figure 8a). It exhibits high-gravity anomalies at the western and northeastern parts(-16.4 mGal), but the northern and southeastern part reveals low-gravity anomalies (-70mGal).

Gravity Separation: The regional-residual separation technique was carried out to filter the regional component, which was related to deep-seated sources and residual component, which was related to local sources. In the present study, authors used least squares technique to apply the gravity separation, calculations for different order up to the fifth order to estimate the best order of separation as shown in (Figure 8b to k).

The correlation factor was calculated for every two successive orders such as the correlation factor for first and second order (r1 - 2). Table 1 show that the best order for gravity separation is the fourth order.

Gravity Interpretation: The fourth-order residual gravity map was used for gravity interpretation to detect the structural elements that dissect study area and controlled for the geometry of the groundwater aquifers. The fault map, as shown in (Figure 9a to b), shows different fault elements of different directions such as NE-SW trend parallel to Gulf of Aqaba, NW-SE trend parallel to the Gulf of Suez and E-W trend parallel to the Mediterranean Sea and the depth for theses structural trends by using Euler decovolution.

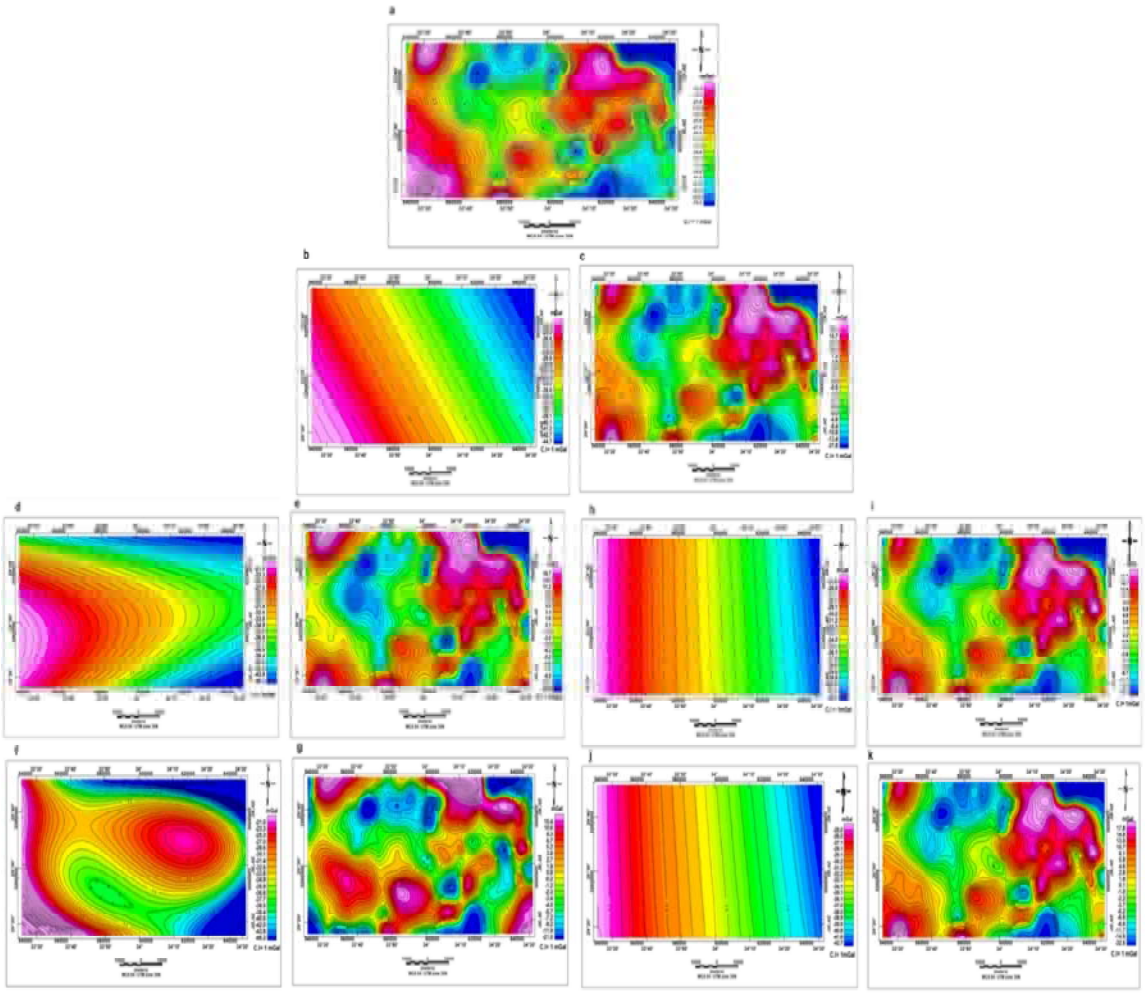

Fig. 8: (a) Bouger anomaly map, (b) First-order regional Bouger anomaly map, (c) First-order residual Bouger anomaly map, (d) Second-order regional Bouger anomaly map, (e) Second-order residual Bouger anomaly map, (f) Third-order regional Bouger anomaly map, (g) Third-order residual Bouger anomaly map, (h) Fourth-order regional Bouger anomaly map, (I) Fourth-order residual Bouger anomaly map, (j) Fifth-order regional Bouger anomaly map, (k) Fifth-order residual Bouger anomaly map

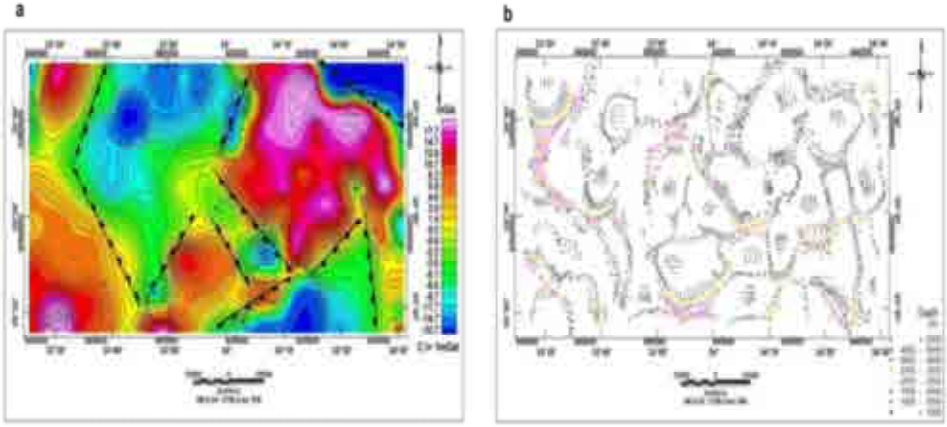

Fig. 9: (a) Fault elements dissecting study area from gravity interpretation. (b) Euler map

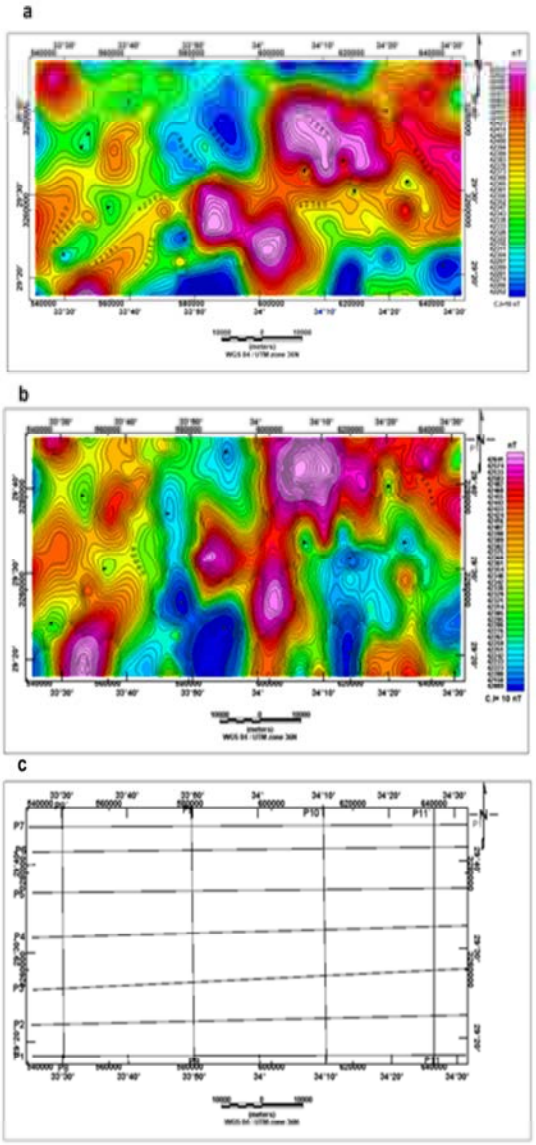

Fig. 10: (a) Total intensity magnetic map. (b) Total intensity magnetic map reduced to the pole (c) Magnetic profiles map

Magnetic Measurements and Interpretation: Ground magnetic have been measured through 200 land stations using Envi-mag proton magnetometer of sensitivity 1 nT; two instruments were used one for field work measurements and the other one for base station recording to estimate diurnal variation correction; after carrying out the necessary reductions as IGRF correction was done for magnetic data which gridded and contoured by using the Geosoft program, 2007 (processing and mapping system) to give the total magnetic intensity map as shown in (Figure 10a). In order to overcome this distortion in the appearance of an anomaly, which depends on the magnetic latitude of the survey area and on the dip angle of the magnetization vector in the body, a mathematical procedure is adopted on a grid values for the contour map of the total magnetic intensity.

Magnetic Interpretation

Reduction to the Pole: Therefore, we begin the interpretation of the magnetic data with the conversion of the total intensity map into a more interpretable map and then reduced to magnetic pole map using magnetic inclination 43.12°, magnetic declination 2.66° and total field strength 42907 nT. This mathematical procedure was first described by [12-15].

The final picture is the total intensity map reduced to the pole as shown in (Figure 10b). Total intensity magnetic map was used for magnetic interpretation to estimate depth to the basement rocks through eleven two-dimensional (2-D) magnetic modeling as shown in (Figure 10c). 2-D magnetic modeling East- West and North- south directions to estimate the topography of the basement surface, also depth to the basement surface which leads to the thickness of aquifer layer through the study area. In all models the basement complex is composed of massive granite of 2.67 gm/cm³ density and magnetic susceptibilities of 0.00535 cgs and the sedimentary cover is presented by sandstone of density 2.39 gm/cm³.

Two Dimensional Gravity/Magnetic Modeling Total intensity magnetic map reduced to the pole was used for magnetic interpretation to estimate depth to the basement rocks through eleven two-dimensional (2-D) gravity/ magnetic modeling as shown in (Figure 11).

The intersection points of profiles (P_1- P_1`, $P_2$- $P_2$`, P_3- P_3`, $P_4$ -$P_4$`, P_5- P_5`, $P_6$- $P_6$` and P_7- P7`) of E-W direction with other profiles, ($P_8$- $P_8$`, P_9- P_9`, $P_{10}$- $P_{10}$` and P_{11}- P_{11}`) of N-S direction, were taken as indicators during the construction of gravity/magnetic modeling as shown in (Figure 10c).

The basement depths obtained along different magnetic profiles are useful to recognize the configuration of the basement topography. The results of 2-D magnetic modeling were used to construct basement relief map (Figure 12), which reflects shallow depth of the basement surface at the Far East region of the area extending from north to south reaching 2400m, also at the northern reaching 2400m and 2100m at the southwestern regions of the area. Also it reflects an increasing depth of the basement surface, mainly at the middle region of the area extending to 4300m below the surface and decreases slightly towards east to 3700m below the surface.

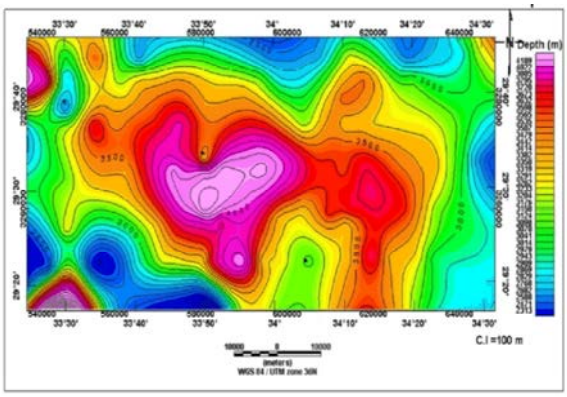

Fig. 12: Basement relief map

DISCUSSION

The results obtained from the interpretation of VES stations 2, 11, 20 and 23 are compatible with results of boreholes Jica 1, 2, 6 and 4 as shown in (Figure 5). The fault elements which delineated through Euler decovolution for gravity data are similar to obtained from the residual gravity anomaly map (Figure 9). The hydrochemistry of borehole Jica1, 2 and 4 indicated the water quality is fresh water which are compatible with resistivity values of Nubian sandstone aquifer which ranging from 109-522 Ohm.m.

Also, the results of 2-D gravity and magnetic modeling are compatible. The correlation between Geoelectrical cross-sections along profiles P1, P2, P3 and P4 compared with gravity profiles indicated that there are conformation for the locations and downthrown of fault elements which delineated from gravity profiles and geoelectrical cross-section (Figure 6).

CONCLUSION

The groundwater is available in central Sinai from a variety of water-bearing formations; each of them has its characteristic geological and hydrogeological conditions which obtained from the drilled wells in the studied area, but the aquifer of our interest is the deeper aquifer which represented by the Nubian sandstone deposits of Lower Cretaceous age . The Lower Cretaceous aquifer is represented by the Nubian sandstone deposits (Malha Formation).This formation has composed mainly of sandstones intercalated with shale and claystone beds. It is corresponding to the geoelectrically identified sixth layer as indicated from (JICA-1). This layer exhibits higher resistivity values ranging from 109 Ohm-m to 522 Ohm-m.

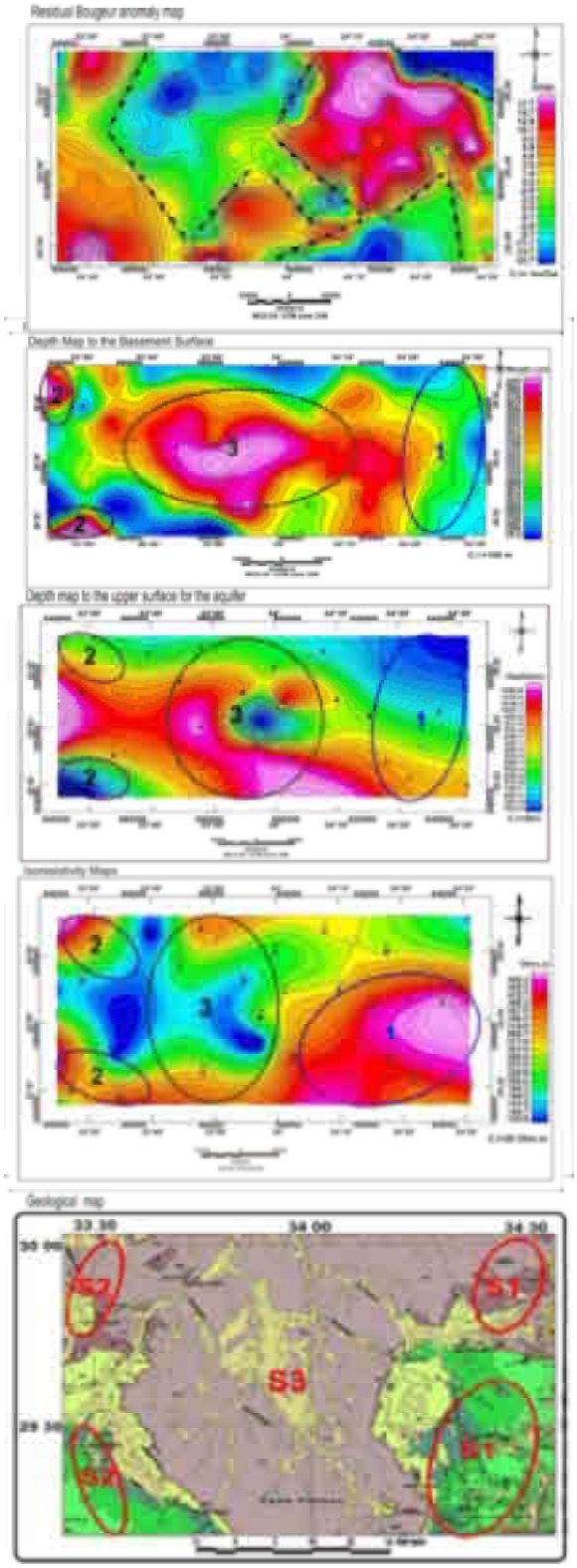

Fig. 13: Integrated geophysical interpretation for groundwater exploration in the studied area

The relatively higher resistivity values exhibited by this aquifer may be attributed to low to moderate salinity, where the TDS recorded in this aquifer is about 1206 ppm.

The upper surface of this layer has been detected at all stations at variable depths ranging from 483 m to 1079 m, but its base cannot be reached with the applied techniques. Then we construct 2-D gravity/ magnetic modeling through East- West and North- south directions to estimate the topography and depth of the basement surface.

The combination of depth to the upper surface of the six layers and the depth to the basement relief reveals that the thickness of the water bearing formation varies from 2000m to 2500m. From structural point of view, the structural elements that dissect study area and controlled for the geometry of the groundwater aquifers. These trends such as NE-SW trend parallel to Gulf of Aqaba, NW-SE trend parallel to the Gulf of Suez and E-W trend parallel to the Mediterranean Sea and the depth for theses structural trends by using Euler decovolution improved the groundwater potentialities of the existing aquifers through the infiltration of the local rainfall and surface floods. The basement depths obtained along different magnetic profiles are useful to recognize the configuration of the basement topography. The basement relief map which reflects shallow depth of the basement surface at the Far East region of the area extending from north to south reaching 2400m, also at the northern reaching 2400m and 2100m at the southwestern regions of the area. Also it reflects an increasing depth of the basement surface, mainly at the middle region of the area extending to 4300m below the surface and decreases slightly towards east to 3700m below the surface. So the priorities for drilling as shown in (Figure 13).

Groundwater is one of the most valuable natural resource for water supplies especially in areas far from surface water channels as the present studied area. So Coupling of the gravity, electrical resistivity and magnetic techniques has succeeded in resolving the subsurface structural conditions of the area.

REFERENCES

1. Nabighian, M.N. and J.C. Macnae, 1991. Time-domain electromagnetic prospecting methods, in Nabighian, M. N. Ed. Electromagnetic Methods in Applied Geophysics, Vol. 2. Society of Exploration Geophys. pp: 427-520.
2. Telford, W.M., L.P. Geldart and R.E. Sheriff, 1995. Applied geophysics. Cambridge University Press, New York.
3. Zohdy, A.R., G. Eaton and D. Mabey, 1974. Application of surface geophysics to water investigations: Techniques of water resources investigation of the United States Geological Survey, Book 2, Chapter D1, pp: 116.
4. Ibrahim, E.H., M.R. Shereef, A.A. El-Galladi and L.B. Pederson, 2004. Geoelectric study on Quaternary groundwater aquifer in northwestern Sinai, Egypt. EGS. J., 2(1): 69-74.
5. Monteiro Santos, F.A.M., S.A. Sultan, R. Patricia and A.L. El-Sorady, 2006. Joint inversion of gravity and geoelectrical data for groundwater and structural investigation: application to the northwestern part of Sinai, Egypt. Geophys, J. Int., 165: 705-718.
6. Sultan, S.A., H.M. Mekhemer, F.A.M. Santos and M. Abd Alla, 2009. Ground water exploration and evaluation by using geophysical interpretation (Case study: Al Qantara East, North Western Sinai, Egypt). Arab, J. Geosci., 2: 199-211.
7. El-Hinnawi, E.M. and Y. Samy, 1995. Textural and mineralogical characteristics of coastal sediments along the Gulf of Aqaba, Sinai: Abstract 4th conf. geol. of Sinai for development, Ismailia.
8. JICA 1992. North Sinai groundwater resources study in the A. R. E: Final report submitted to the Research Institute for Water Resources, Ministry of Public Works and Water Resources, Cairo, Egypt.
9. Bobachev, A., I. Modin and V. Shevnin, 2001. IPI2WIN v.2.0, User's Manual.
10. Chuansheng, W., H. Jinrong, and Z. Xiufen, 2008. A genetic algorithm approach for selecting tikhonov regularization parameter. IEEE Congress on Evolutionary Computation (CEC 2008).
11. Gian, P.D., B. Ernesto and M. Cristina, 2003. Inversion of electrical conductivity data with Tikhonov regularization approach: some considerations. Ann Geophys. 46: 3.
12. Baranov, V., 1957. A new method for interpretation of aeromagnetic maps: pseudo-gravimetric anomalies. Geophys. 22: 359-383.
13. Baranov, V., 1975. Potential fields and their transformation in applied geophysics. Geoexploration Monographs, series 1-6, Gebrüder, Borntraeger, Berlin-Stuttgart.
14. Baranov, V. and H. Naudy, 1964. Numerical calculation of the formula of reduction to the magnetic pole. Geophys. 29: 67-79.
15. Bhattacharyya, B.K., 1965. Two dimensional harmonic analysis as a tool for magnetic interpretation. Geophys. 30(5): 829-857.